Geophysical Research Letters

RESEARCH LETTER
10.1029/2026GL121983

Barium Isotopes Indicate Spatiotemporal Heterogeneity of Marine Primary Productivity During the Toarcian Oceanic Anoxic Event

Wenhan Chen[1,2], David B. Kemp[3], Hugh C. Jenkyns[4], Stuart A. Robinson[4], Yibo Lin[5], Jun Hu[1,2], Zhong Han[6], Tianchen He[7], Feifei Zhang[5], Xilei Sun[3], Guangyu Shi[8], and Chao Li[1,2]

[1]State Key Laboratory of Oil and Gas Reservoir Geology and Exploitation & Institute of Sedimentary Geology, Chengdu University of Technology, Chengdu, China, [2]International Center for Sedimentary Geochemistry and Biogeochemistry Research, Chengdu University of Technology, Chengdu, China, [3]State Key Laboratory of Geomicrobiology and Environmental Changes and Hubei Key Laboratory of Critical Zone Evolution, School of Earth and Planetary Sciences, China University of Geosciences, Wuhan, China, [4]Department of Earth Sciences, University of Oxford, Oxford, UK, [5]School of Earth Sciences and Engineering, Nanjing University, Nanjing, China, [6]State Key Laboratory of Palaeobiology and Stratigraphy, Nanjing Institute of Geology and Palaeontology, Chinese Academy of Sciences, Nanjing, China, [7]College of Oceanography, Hohai University, Nanjing, China, [8]Wuhan SampleSolution Analytical Technology Co., Ltd, Wuhan, China

Abstract The Toarcian Oceanic Anoxic Event (T-OAE, ~183 Ma) was characterized by globally enhanced organic-carbon burial and a negative carbon-isotope excursion (N-CIE). However, the role of marine productivity at this time, and its spatiotemporal variability, is unclear. We present the first carbonate barium-isotope ($\delta^{138}Ba_{carb}$) records across the T-OAE from a shallow-water platform (Nianduo, SE Tethys) and a pelagic basin (Dogna, Alpine-Mediterranean Tethys) to reconstruct productivity dynamics. Both sites show positive $\delta^{138}Ba_{carb}$ shifts at the N-CIE onset, indicating supra-regional productivity enhancement. At Nianduo, $\delta^{138}Ba_{carb}$ rises through the onset, consistent with increased export production driven by weathering-derived nutrient inputs. At Dogna, $\delta^{138}Ba_{carb}$ declines within the N-CIE onset due to reduction-driven barite dissolution, followed by a rise during the N-CIE recovery. The Dogna data suggest protracted elevation of pelagic productivity supported by nutrient upwelling and aeolian fertilization. As such, pelagic basins may have acted as an important carbon sink regulating the T-OAE carbon cycle.

Plain Language Summary During the Early Jurassic Toarcian Oceanic Anoxic Event, large areas of the ocean became oxygen-poor, allowing more organic carbon to be buried in sediments and altering Earth's carbon cycle. By studying barium-isotope records preserved in marine limestones from a shallow platform in China and a deep-sea basin in Italy, we find that ocean productivity increased at the beginning of the event across a wide region. However, this increase did not persist everywhere. Productivity on the shallow platform declined relatively quickly, whereas the deep basin continued to support high productivity for a much longer time. This sustained high productivity in deeper waters likely helped store large amounts of carbon in marine sediments. Our results show that deep-sea basins can play a particularly important role in regulating carbon burial during periods of extreme climate and environmental change.

Key Points:

- Carbonate Ba isotopes reveal sustained high pelagic productivity relative to the neritic setting during the Toarcian Oceanic Anoxic Event
- Upwelling, anoxia-driven P recycling, and aeolian fertilization jointly fueled the pelagic productivity
- Pelagic basins acted as a key carbon sink, assisting in the regulation of the carbon cycle during the Toarcian Oceanic Anoxic Event

Supporting Information:

Supporting Information may be found in the online version of this article.

Correspondence to:

D. B. Kemp and C. Li,
davidkemp@cug.edu.cn;
chaoli@cdut.edu.cn

Citation:

Chen, W., Kemp, D. B., Jenkyns, H. C., Robinson, S. A., Lin, Y., Hu, J., et al. (2026). Barium isotopes indicate spatiotemporal heterogeneity of marine primary productivity during the Toarcian Oceanic Anoxic Event. *Geophysical Research Letters*, *53*, e2026GL121983. https://doi.org/10.1029/2026GL121983

Received 22 JAN 2026
Accepted 28 APR 2026

Author Contributions:

Conceptualization: Wenhan Chen, David B. Kemp, Chao Li
Data curation: Wenhan Chen, Yibo Lin, Jun Hu, Xilei Sun, Guangyu Shi
Funding acquisition: Wenhan Chen, David B. Kemp, Chao Li
Investigation: Wenhan Chen, David B. Kemp, Chao Li
Methodology: Wenhan Chen, Hugh C. Jenkyns, Stuart A. Robinson, Yibo Lin, Jun Hu, Feifei Zhang, Xilei Sun, Guangyu Shi
Resources: Hugh C. Jenkyns, Stuart A. Robinson, Zhong Han
Validation: Wenhan Chen, Feifei Zhang

1. Introduction

The early Toarcian Oceanic Anoxic Event (T-OAE, ~183 Ma) represents one of the major climatic and environmental disruptions of the Early Jurassic (Jenkyns, 1988). The event was marked by an abrupt negative carbon-isotope excursion (N-CIE) globally recognized in both organic and inorganic carbon archives and typically dissecting an overarching positive anomaly (Jenkyns, 2010). The positive excursion is related to an increase in global burial of reduced carbon (Jenkyns, 1988), whereas the negative excursion results from the massive release of ^{13}C-depleted carbon into the biosphere (Hesselbo et al., 2000). This carbon release is commonly linked to the emplacement of the Karoo–Ferrar large igneous provinces via degassing of volcanogenic CO_2 (Pálfy & Smith, 2000) and was associated with global warming and a suite of environmental disturbances, including widespread deposition of organic-rich black shales, oceanic deoxygenation locally to the point of euxinia, ocean acidification, enhanced continental and submarine weathering and hydrological cycling (Gambacorta et al., 2024; Jenkyns, 2010; Kemp, Han, et al., 2024; Kemp, Suan, et al., 2022). Elevated marine primary productivity (the rate of conversion of inorganic carbon into organic carbon (OC) in the surface ocean) and the associated increase in

Visualization: Wenhan Chen, Zhong Han, Chao Li
Writing – original draft: Wenhan Chen
Writing – review & editing: David B. Kemp, Hugh C. Jenkyns, Stuart A. Robinson, Yibo Lin, Jun Hu, Zhong Han, Tianchen He, Feifei Zhang, Xilei Sun, Chao Li

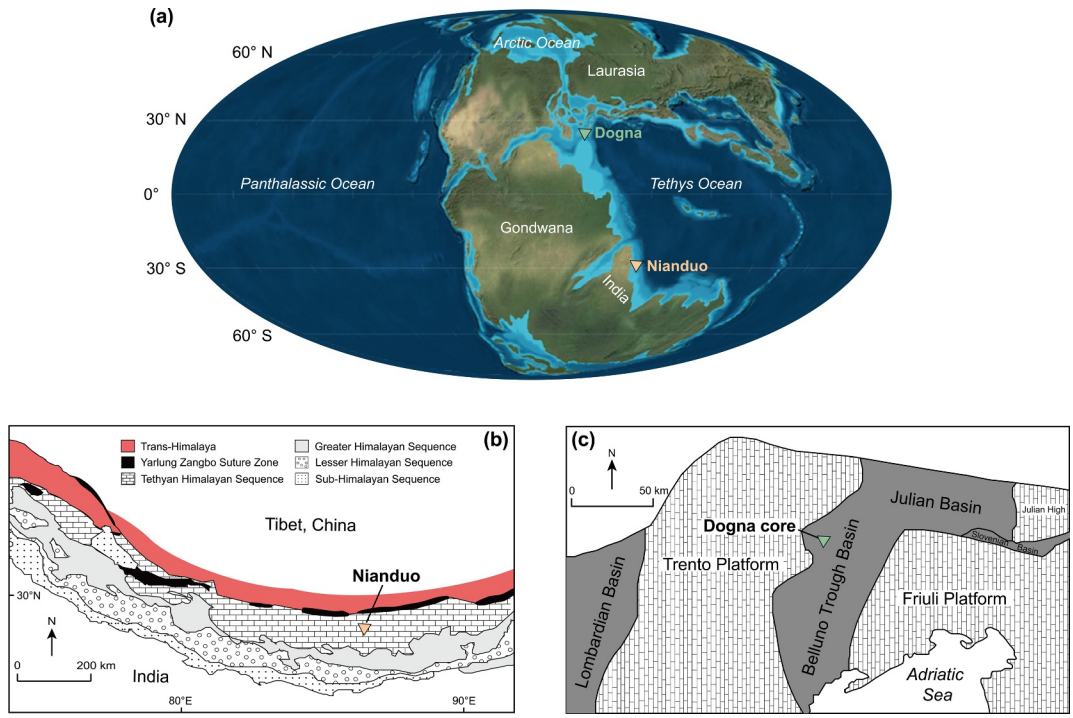

Figure 1. Geological setting of the two study sites. (a) Paleogeographic map showing the locations of the Dogna core (green triangle) and Nianduo section (yellow triangle) in the Early Jurassic (after Han et al., 2018). (b) Map of the Himalayan area (SE Tethys), showing the regional sedimentary sequences and the site of the Nianduo section (after Han et al., 2018). (c) Configuration of Early Jurassic carbonate platforms and basins in the Alpine area (NW Tethys), with the Dogna core shown in the Belluno Trough Basin (after Ettinger et al., 2021).

export production (the flux of particulate OC from the surface ocean to depth) are key drivers of OC burial (Pedersen & Calvert, 1990). However, the spatiotemporal variability of marine productivity during the T-OAE remains poorly constrained, hindering a better understanding of how productivity regulated OC burial and consequently shaped climatic and environmental trajectories over this critical period. Much of this uncertainty stems from proxy limitations (Text S1 in Supporting Information S1) and the scarcity of deep-sea records.

Seawater barium isotopes ($\delta^{138}Ba_{sw}$) are a promising tool to track marine Ba cycling and, by extension, productivity (e.g., Bridgestock et al., 2019; Zhang et al., 2025). The quasi-nutrient type distribution of marine Ba ([Ba]) and $\delta^{138}Ba_{sw}$ in the modern ocean is primarily controlled by biogenic barite formation during microbial remineralization of sinking OC and partial dissolution of barite at depth via microbial sulfate reduction (MSR) (Horner et al., 2015; Figure S1 in Supporting Information S1). Barite precipitation from seawater imposes a significant isotopic fractionation (−0.5 to −0.4‰), in contrast to negligible fractionation during dissolution. Enhanced surface productivity thus increases Ba export, lowering surface [Ba] and elevating surface $\delta^{138}Ba_{sw}$ (Horner et al., 2015; Hsieh & Henderson, 2017). Previous work indicates growth rate-dependent Ba-isotopic fractionation for aragonite and negligible fractionation for calcite and witherite (Mavromatis et al., 2016, 2018). Thus, properly screened limestones can preserve primary $\delta^{138}Ba_{sw}$ signals, allowing the reconstruction of marine primary productivity.

To investigate the spatiotemporal response of marine productivity during the T-OAE, we present the first carbonate $\delta^{138}Ba$ ($\delta^{138}Ba_{carb}$) records across this event from two Tethyan successions with widely differing depositional environments (Figure 1a): one deposited on a shallow-water carbonate platform (Nianduo section in southern China, SE Tethys; Figure 1b), and the other in a basinal pelagic environment (Dogna core in northern Italy, Alpine-Mediterranean Tethys; Figure 1c). At both sites, biostratigraphy and carbon isotopes ($\delta^{13}C$) have constrained the T-OAE (defined for our purposes by the N-CIE) stratigraphically (Han et al., 2018; Jenkyns et al., 1985, 2001). Whole-rock mercury (Hg) concentrations, Fe- and P-speciation data were also obtained at Dogna to track local redox and nutrient availability. Detailed information on geological setting is provided in Text S2 in Supporting Information S1.

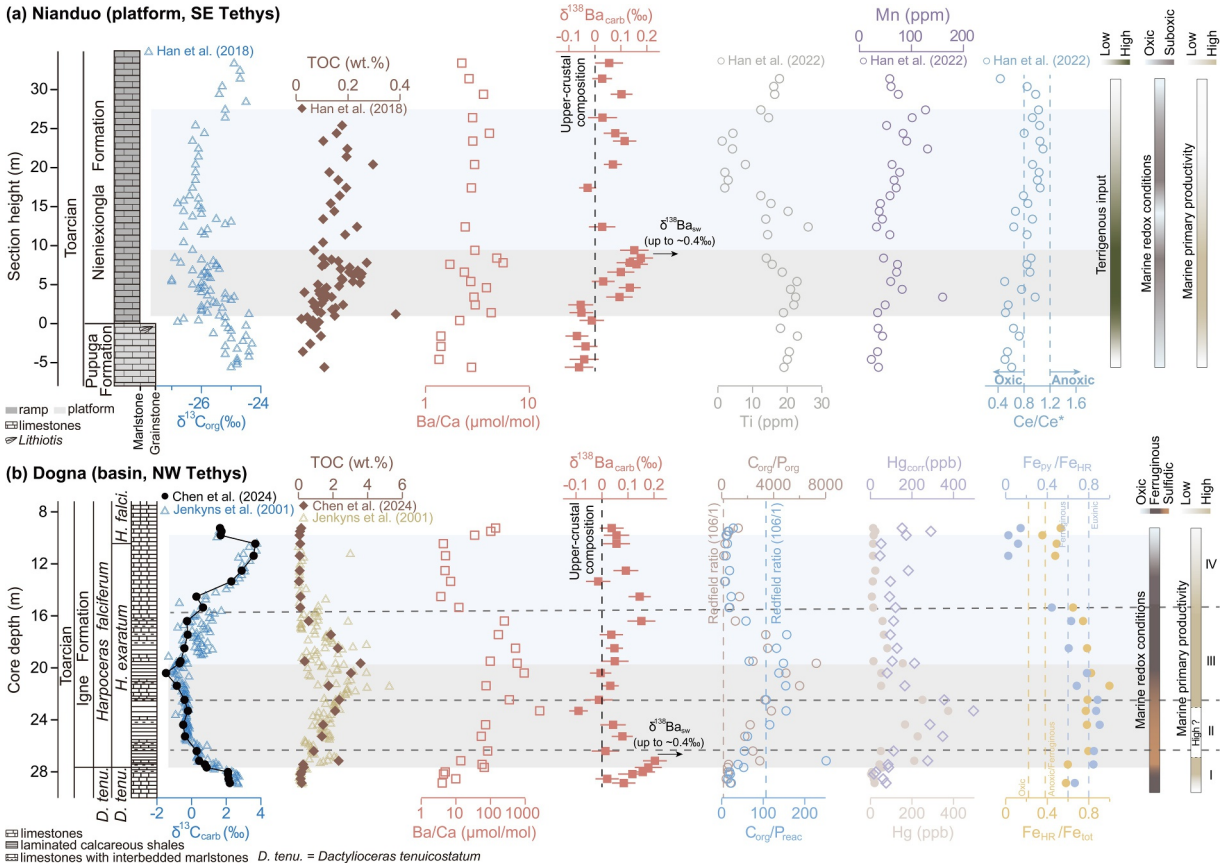

Figure 2. Litho- and bio-stratigraphy, geochemical data, and inferred weathering, redox, and productivity at Nianduo (a) and Dogna (b). In panel (a), the weathering bar is constrained by Ti concentration (Han et al., 2022), and the redox bar by Ce anomalies and Mn concentration (Han et al., 2022). In panel (b), the redox bar is based on our Fe-speciation data. Error bars of $\delta^{138}Ba_{carb}$ at both sites represent 2SD analytical uncertainties (Table S1 in Supporting Information S1). Light gray bar, N-CIE onset; Light blue bar, N-CIE recovery.

2. Materials and Methods

At Nianduo, 24 bulk carbonate samples spanning the N-CIE were analyzed for carbonate-hosted elemental concentrations and $\delta^{138}Ba_{carb}$. The selected samples are a subset of samples of which the carbon isotopes from both organic and inorganic carbon archives and oxygen and strontium isotopes from bulk carbonate rocks ($\delta^{18}O_{carb}$ and $^{87}Sr/^{86}Sr$, respectively) have been previously published (Han et al., 2018; Yang et al., 2024).

At Dogna, 28 samples were analyzed for whole-rock elemental concentrations, Hg concentrations, P-speciation, and carbonate-hosted elemental concentrations. Previously published $\delta^{13}C_{carb}$ data of these 28 samples have shown a complete N-CIE morphology (Chen et al., 2024; Figure 2b). Out of these 28 samples, 23 samples were analyzed for $\delta^{138}Ba_{carb}$. Because Fe-speciation analysis is generally valid for carbonates with total Fe concentrations (Fe_{tot}) of >0.5 wt.% (cf. Clarkson et al., 2014), 15 samples (Fe_{tot} > 0.5 wt.%) were selected.

P-speciation and Hg concentrations were not analyzed at Nianduo, given the generally low TOC (mostly <0.2 wt%, Figure 2a; Han et al., 2018), and because OC in sediments is typically one of the major hosts of P and Hg (Froelich et al., 1979; Grasby et al., 2019). Similarly, because of the generally low Fe_{tot} (mostly <0.1 wt.%; Han et al., 2018), Fe-speciation analysis was also not performed at Nianduo.

The analyses of carbonate-hosted $\delta^{138}Ba$ and major and trace elements were based on the methods of Lin et al. (2020) and conducted at Nanjing University. Fe- and P-speciation analyses follow Jin et al. (2016) and Thompson et al. (2019), respectively, and were conducted at Chengdu University of Technology. Whole-rock Hg concentrations were analyzed following Hua et al. (2023) at China University of Geosciences (Wuhan).

Because elevated $CaCO_3$ proportions can artificially depress bulk Hg and TOC concentrations (i.e., dilution effect) without reflecting changes in Hg input, burial, or OC accumulation (cf. Fendley et al., 2024), we corrected the bulk Hg and TOC concentrations of the Dogna samples (given considerably varying $CaCO_3$ contents, ranging from 23.5 wt.% to 92.3 wt.% at this site; Chen et al., 2024; Figure S2 in Supporting Information S1) to a carbonate-free basis via:

$$X_{corr} = X/(1–CaCO_3/100)$$

where X denotes the bulk concentrations of Hg or TOC, X_{corr} denotes the corrected carbonate-free concentrations, and $CaCO_3$ is the weight percent of calcium carbonate in a particular sample. Note that because these corrected values are normalized to the non-carbonate fraction, they are referred to hereafter as carbonate-free OC (OC_{corr}) rather than bulk TOC. All analytical protocols and data sets are provided in Text S3 and Table S1 in Supporting Information S1.

3. Results and Discussion

3.1. Preservation of Geochemical Signals

To minimize potential detrital contamination, all samples were treated with mild acid (1 M acetic acid) following sequential leaching protocols (Lin et al., 2020) before Ba purification. Extremely low Al content (average 0.01 wt.% at Nianduo and 0.05 wt.% at Dogna) and Al/Ca molar ratio (average 0.0005 mol/mol at Nianduo and 0.006 mol/mol at Dogna) suggest negligible detrital contamination during Ba extraction.

Carbonate mineralogical alteration can influence $\delta^{138}Ba_{carb}$ signatures, particularly during aragonite–calcite transformation (Lin et al., 2022). However, petrographic observations show that the carbonate rocks at both sites are primarily composed of calcite (Bellanca et al., 1999; Farrimond et al., 1994; Han et al., 2016, 2018). Moreover, systematic trends can be expected between $\delta^{138}Ba_{carb}$ and both Mg/Ca and Sr/Ca if the mineral transformation (from aragonite to calcite) has played a major role in altering the $\delta^{138}Ba_{carb}$ values (e.g., Zhang et al., 2024). However, the lack of any significant correlations between $\delta^{138}Ba_{carb}$ and both Sr/Ca and Mg/Ca molar ratios at either site (Figure S3 in Supporting Information S1) suggests limited impacts of such mineral transformation on our $\delta^{138}Ba_{carb}$ data.

Due to generally high $\delta^{18}O$ (>−5‰) of our analyzed Dogna samples (Chen et al., 2024), meteoric diagenesis (i.e., a late diagenetic process with freshwater involved, characterized by depleted $\delta^{18}O$) may well have been negligible. Nevertheless, the abnormally high Ba/Ca ratios at Dogna (average 225 μmol/mol), compared to those at Nianduo (average 3 μmol/mol), may indicate additional Ba incorporation during diagenesis at this pelagic site. This possibility is supported by the occurrence of manganese carbonates in certain intervals at Dogna, indicating fluctuating redox conditions and Mn recycling during early diagenesis (e.g., Bellanca et al., 1999; Jenkyns et al., 1991). Importantly, however, $\delta^{138}Ba_{carb}$ values from the Dogna core do not show any significant correlations with Mn/Sr molar ratios, nor with other commonly used diagenetic indicators (e.g., Sr concentrations and $\delta^{18}O_{carb}$; Jacobsen & Kaufman, 1999; Figure S5 in Supporting Information S1). These data suggest that Mn-related diagenesis at Dogna exerted only a limited influence on our $\delta^{138}Ba_{carb}$ record. Moreover, stratigraphically adjacent OC-rich marlstone and manganese limestone have similar $\delta^{138}Ba$ values (e.g., 28.01–27.66 m and 19.49–17.45 m; Figure 2b). This consistency across lithologies suggests that local diagenetic overprints were probably minimal with respect to $\delta^{138}Ba_{carb}$.

At Nianduo, minor diagenetic overprints may have occurred locally, as indicated by unusually high $^{87}Sr/^{86}Sr$ values at some horizons (Yang et al., 2024). However, diagenesis at this site has been rigorously evaluated petrographically. Only the oolitic limestones and micrites with no clear diagenetic overprints were selected for high-resolution geochemical analyses (Han et al., 2018, 2022; Yang et al., 2024). Accordingly, samples exhibiting anomalously high $^{87}Sr/^{86}Sr$ values were excluded from this study. Representative photomicrographs of the analyzed samples (Figure S4 in Supporting Information S1) further confirm insignificant recrystallization. In addition, relatively higher $\delta^{18}O_{carb}$ values (>−10‰) and a negligible correlation between $\delta^{13}C_{carb}$ and $\delta^{18}O_{carb}$ ($R^2 = 0.005$) argue against significant meteoric alteration at this shallow-water site (Han et al., 2018). Consistent with these previous diagenetic evaluations, $\delta^{138}Ba_{carb}$ at Nianduo exhibits insignificant correlations with Sr

concentrations, Mn/Sr molar ratios, or $\delta^{18}O_{carb}$ (Figure S5 in Supporting Information S1), further supporting minimal diagenetic impacts on our $\delta^{138}Ba_{carb}$ record.

Consistently low Mg/Ca molar ratios (average 0.02 at Nianduo and 0.06 at Dogna; Table S1 in Supporting Information S1) argue against significant dolomitization at either site, in agreement with previous thin-section observations (Bellanca et al., 1999; Han et al., 2016, 2018). The limited extent of dolomitization at Dogna therefore suggests that our Fe-speciation data can potentially track the local bottom-water redox state (cf., Clarkson et al., 2014). Meanwhile, rapid deposition (e.g., turbidites) and the delivery of intensely weathered sediments from mountainous regions—capable of bypassing inner-shelf settings that typically act as a major trap for Fe (oxyhydr)oxide minerals—may also impact Fe-speciation records, thereby biasing the interpretation of local redox conditions (Canfield et al., 1996; Wei, Chen, et al., 2021). However, the Dogna site was deep water (>1,000 m; Bosellini et al., 1981), far from major landmasses, and there was an absence of turbidites, suggesting limited impacts from these two factors on our Fe-speciation records as a paleo-redox tracer. P-speciation analyses show a strong correlation ($R^2 = 0.95$, *p-value* < 0.001; Figure S6A in Supporting Information S1) between bulk P concentrations (P_{tot}) measured by the X-ray fluorescence spectrometer (XRF) and the sum of sequentially extracted phases (P_{sum}). This geochemical pattern indicates that our individual P extractions successfully recovered the bulk P concentrations. Although late-stage diagenesis may transfer authigenic apatite (P_{auth}) to more crystalline P-bearing phases (P_{det}) (Thompson et al., 2019), several observations suggest that such redistribution was limited in our samples. P_{det} concentrations are low (average 29 ppm, $n = 28$; Table S1 in Supporting Information S1), falling below typical values for modern sediments (60–600 ppm; Canfield et al., 2020). Additionally, P_{det} covaries positively with Al ($R^2 = 0.68$, *p-value* < 0.001; Figure S6B in Supporting Information S1), indicating that the extracted P_{det} primarily reflects the detrital P input. Thus, while a portion of the P_{auth} pool may have recrystallized and been operationally extracted as P_{det}, our observations suggest that such post-depositional transfer was limited. Importantly, samples deposited under sulfidic conditions, as inferred from our Fe-speciation data (see the discussion below), generally have a C_{org}/P_{tot} molar ratio exceeding the Redfield ratio (Figure S2 in Supporting Information S1), consistent with efficient P recycling under sulfidic conditions and independent of any diagenetic overprints on P partitioning. These multiple lines of evidence collectively indicate that our samples used to investigate marine Ba cycling, redox conditions, and nutrient availability preserve primary seawater signatures.

3.2. Spatiotemporal Heterogeneity of Marine Productivity During the T-OAE

3.2.1. Shallow-Water Carbonate-Platform Environment (Nianduo)

At the shallow-water Nianduo section, $\delta^{138}Ba_{carb}$ increased by +0.30‰ at the N-CIE onset (Figure 2a), well above our analytical uncertainty of approximately ±0.05‰ (2SD; Table S1 in Supporting Information S1). Although globally enhanced continental weathering and hydrological cycling at the T-OAE N-CIE onset (e.g., Kemp, Han, et al., 2024) could have increased riverine Ba to shallow-marine settings such as Nianduo, Ba-isotope constraints indicate that this effect was limited. Specifically, assuming a −0.21‰ offset between bulk carbonates and ambient seawater (Lin et al., 2022), reconstructed $\delta^{138}Ba_{sw}$ reaches 0.40‰ at Nianduo (Figure 2a), which exceeds the isotopic composition of typical river-dissolved loads (0.10–0.35‰, mean 0.22‰; Bridgestock et al., 2021 and references therein) and thus is inconsistent with dominant riverine control. Moreover, estuarine desorption would drive net riverine Ba toward upper-crustal composition (Bridgestock et al., 2021), approximating 0.00‰ (Nan et al., 2018), thereby dampening any positive isotopic influence. The observed +0.30‰ increase in $\delta^{138}Ba_{carb}$ through the N-CIE onset interval therefore most logically reflects increased formation of biogenic barite linked to elevated productivity. The subsequent isotopic decline during the N-CIE recovery interval indicates reduced export production, as generally oxic/suboxic conditions at Nianduo (Han et al., 2022) would have inhibited substantial MSR-driven barite dissolution and release of isotopically lighter Ba.

3.2.2. Pelagic Deep-Marine Basinal Environment (Dogna)

Because sulfidic conditions can significantly influence barite preservation by regulating MSR (Schoepfer et al., 2015), we employ Fe-speciation to interpret depositional redox at Dogna and further evaluate its role in local Ba cycling. Note that we here demarcate the Dogna succession into four stages based on the variations of $\delta^{138}Ba_{carb}$ (see Stage I–IV in Figure 2b) for further discussion below. In both modern and ancient marine depositional settings, redox conditions can be evaluated using the ratio of highly reactive Fe (Fe_{HR}) to Fe_{tot}.

Values exceeding 0.38 are generally interpreted to reflect anoxic conditions, whereas values below 0.22 indicate oxic environments, with values between considered equivocal. When anoxia is indicated, the extent of pyritization (Fe_{PY}) of the Fe_{HR} pool is further employed to distinguish ferruginous ($Fe_{PY}/Fe_{HR} < 0.6$) from sulfidic conditions ($Fe_{PY}/Fe_{HR} > 0.6$–0.8) (Poulton, 2021). On this basis, our Fe-speciation data indicate that ferruginous bottom waters with intermittent sulfidic conditions prevailed at Dogna from the N-CIE onset through the middle recovery phase (Figure 2b), though the occurrence of manganese carbonates at some horizons likely suggests fluctuating episodes (e.g., Bellanca et al., 1999; Jenkyns et al., 1991). This marine geochemistry reflects active MSR, which should have favored barite dissolution and the resulting release of isotopically lighter Ba to bottom waters, leading to lower $\delta^{138}Ba_{sw}$. This decreasing trend could have been amplified, given a globally low-sulfate ocean during the T-OAE (<8 mM vs. 29 mM in modern ocean) inferred from multiple sulfate sulfur-isotope records across Europe and China (e.g., Gill et al., 2011; Newton et al., 2011) that likely suppressed barite formation (as observed in pre-Cambrian oceans with extremely low sulfate, <1 mM; Wei, Ling, et al., 2021). However, a +0.20‰ shift in $\delta^{138}Ba_{carb}$ at the N-CIE onset at Dogna (Stage I), together with a similar +0.30‰ shift at Nianduo, indicates that sulfate availability did not control the Ba-isotope signal.

Moreover, model simulations indicate globally reduced oceanic circulation during the T-OAE (Dera & Donnadieu, 2012). Consequently, the efficiency of basin- to global-scale lateral homogenization of surface $\delta^{138}Ba_{sw}$ (as observed in the modern oceans; cf. Yu et al., 2022) may have been diminished. Given the substantial paleogeographic separation and contrasting depositional settings of our two study sites (Figure 1), such weakened connectivity would have favored the preservation of regional isotopic signatures. Increased volcanogenic dust and associated aeolian Ba inputs due to the emplacement of Karoo–Ferrar large igneous provinces are also unlikely to explain the positive $\delta^{138}Ba_{carb}$ shift at Dogna because aeolian $\delta^{138}Ba$ (0.01‰; Mayfield et al., 2024) is comparable to upper-crustal composition and far lower than the observed $\delta^{138}Ba_{carb}$ (up to 0.2‰). Thus, at Dogna, the positive $\delta^{138}Ba_{carb}$ shift, coupled with generally low Ba/Ca at the N-CIE onset (Stage I), reflects increased biogenic barite formation driven by elevated pelagic productivity rather than external Ba inputs. Together with a similar $\delta^{138}Ba_{sw}$ peak at Nianduo (0.40‰), our data indicate that the Ba cycle in the Tethys Ocean during the T-OAE may have resembled that of the present-day Southern Ocean (surface $\delta^{138}Ba_{sw}$ of +0.34‰; Yu et al., 2022), likely marked by comparable export production. Given relatively oxygenated upper waters in Stage I, as inferred from I/(Ca + Mg) and Ce anomalies (Chen et al., 2024; Figure S2 in Supporting Information S1), enhanced preservation of sinking OC in the water column was unlikely to have been the dominant driver of sedimentary OC enrichment. The coeval increase in TOC at Dogna was therefore more consistent with elevated pelagic productivity—as indicated by our Ba data.

A subsequent negative $\delta^{138}Ba_{carb}$ shift in Stage II at Dogna coincides with marked Hg enrichment (Figure 2b). As Hg in the natural environment is derived mainly from magmatic outgassing (Grasby et al., 2019), the anomalous Hg enrichment during this interval most likely reflects increased volcanogenic atmospheric input, particularly given the deep-marine setting and hence minimal terrestrial Hg input (cf. Them et al., 2019). Therefore, enhanced volcanic dust delivery likely contributed to the decreased $\delta^{138}Ba_{carb}$ in Stage II. This inference is supported by elevated sedimentary Hg concentrations reported from multiple globally distributed sections during the T-OAE (Percival et al., 2015; Storm et al., 2024), suggesting a broadly synchronous global volcanogenic signal. Nevertheless, although the abnormally high Ba/Ca values may partly reflect additional Ba incorporation during early diagenesis (see Section 3.1 above), the clear negative correlation between $\delta^{138}Ba_{carb}$ and Ba/Ca during Stage II is best explained by efficient barite dissolution under expanded anoxia, which introduced Ba-rich, isotopically lighter deep waters into the surface, where the signal was ultimately captured during carbonate precipitation—a pattern consistent with the findings during the Late Cretaceous OAE 2 (Zhang et al., 2024). This inference agrees well with the evidence for anoxia with intermittent sulfidic conditions at Dogna through the upper (Chen et al., 2024; Figure S2 in Supporting Information S1) and lower parts of the water column (Figure 2b), supporting preservation-associated OC enrichment following the N-CIE onset. Notably, P-speciation, Hg concentrations (Figure 2), and published $\delta^{15}N$ records (Jenkyns et al., 2001; Figure S2 in Supporting Information S1) collectively indicate enhanced nutrient availability at Dogna during Stage II (see Section 3.3), consistent with potentially elevated pelagic productivity during this interval, which could have, in turn, facilitated the expansion of anoxia via aerobic OC respiration.

Stratigraphically upwards through the decreasing $\delta^{13}C$ interval to the middle N-CIE recovery phase (Stage III), a marked positive $\delta^{138}Ba_{carb}$ shift coincides with decreasing Ba/Ca at Dogna (Figure 2b). This pairing implies increased barite formation driven by elevated pelagic productivity. Indeed, local anoxia with intermittent sulfidic

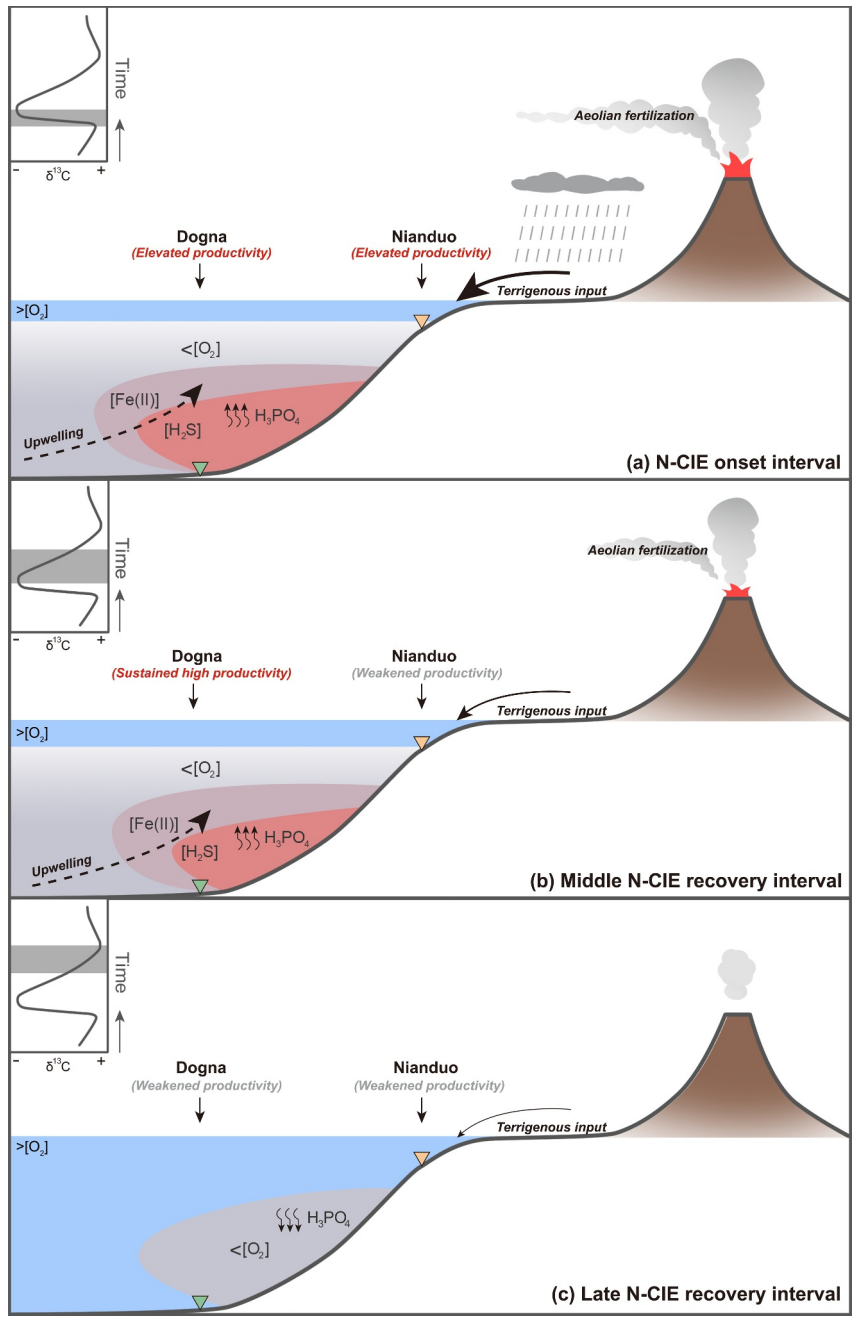

Figure 3. Conceptual model illustrating nutrient availability and productivity heterogeneity during the T-OAE. On the upper left corner of each panel is the idealized $\delta^{13}C$ record through the event, with stratigraphic intervals marked by gray shading representing different phases. Note that the arrow thickness qualitatively represents variations in terrigenous nutrient supply during the T-OAE N-CIE interval.

conditions would have dampened this isotopic signal, implying a larger productivity increase that likely contributed to the coeval OC enrichment. Notably, in contrast to the neritic setting, where elevated surface productivity appears to have been largely restricted to the N-CIE onset interval, pelagic surface waters sustained high productivity well into the N-CIE recovery phase, highlighting pronounced spatiotemporal heterogeneity in productivity evolution (Figures 3a and 3b). In Stage IV, such sustained high pelagic productivity weakened as reflected by decreasing $\delta^{138}Ba_{carb}$ under more oxygenated conditions (Figures 2b and 3c).

Independent evidence, for example, increased sterane abundances at Dogna (Farrimond et al., 1994) and elevated sedimentary Ba concentrations accompanied by abundant radiolarians and fecal pellets at the nearby Longarone section (Bellanca et al., 1999; Jenkyns, 1988), also support elevated pelagic productivity during the T-OAE. However, these sedimentological and paleontological indicators are stratigraphically discontinuous and, together with the interpretive limitations of traditional productivity proxies such as bulk Ba concentrations (Text S1 in Supporting Information S1), cannot resolve the temporal trajectory of pelagic productivity through the event. By contrast, our marine Ba cycling and δ^{138}Ba records provide a more reliable and temporally resolved reconstruction of marine primary productivity. In summary, our Ba-cycle analysis reveals pronounced spatiotemporal heterogeneity in marine primary productivity during the T-OAE.

3.3. Mechanisms Behind and Implications for OC Burial During the T-OAE

At the shallow-water Nianduo site, a marked rise in $^{87}Sr/^{86}Sr$, total rare earth elements, and elements associated with detrital mineral phases (e.g., Ti) at the N-CIE onset indicates increased terrigenous inputs (Han et al., 2022; Yang et al., 2024; Figure 2a), consistent with globally enhanced silicate weathering as inferred from multiple Os-isotope records (Cohen et al., 2004; Kemp et al., 2020; Them et al., 2017). The values of these proxies decline in the recovery phase. The covariations between weathering-driven terrigenous inputs and our δ^{138}Ba-based productivity data suggest terrigenous nutrient availability as a primary driver of shallow-water productivity (Figure 3).

At Dogna, the deep-marine setting and dominantly marine organic matter (Farrimond et al., 1994) indicate limited direct terrestrial particulate input via run-off. Instead, sustained high pelagic productivity is best attributed to active local upwelling of nutrient-rich deeper waters, consistent with the positive δ^{15}N shift reflecting continued supply of upwelled isotopically heavier, partially denitrified nitrate (Jenkyns et al., 2001; Figure S2 in Supporting Information S1). Here, we demonstrate that anoxia-driven P recycling from sediment further amplified this nutrient flux based on P-phase partitioning. This method quantifies four different P-bearing phases, including organic-bound P (P_{org}), Fe (oxyhydr)oxide-bound P (P_{Fe}), biogenic and authigenic apatite (P_{auth}), and detrital P (P_{det}) (Thompson et al., 2019). Reactive P (P_{reac}), which is bioavailable and represents potentially mobile P during transport and early diagenesis, is defined as the sum of P_{org}, P_{Fe}, and P_{auth}. P_{org} is preferentially released from organic matter via remineralization, elevating C_{org}/P_{org} above the Redfield ratio of 106/1, while P_{Fe} can be mobilized during reductive dissolution of Fe (oxyhydr)oxides. A proportion of this recycled P would undergo "sink switching" to authigenic phases, but under sulfidic conditions, it would be efficiently returned to the water column, promoting a strong positive productivity feedback following upwelling to the surface ocean (Paytan & McLaughlin, 2007).

At Dogna, coupled increases in C_{org}/P_{org}, C_{org}/P_{reac}, P_{reac}, and P_{tot} at the N-CIE onset (Figure 2b and Figure S2 in Supporting Information S1) indicate P release during organic-matter degradation and Fe-oxide reduction, with limited sedimentary retention under sulfidic conditions (Figure 3a). Notably, from the late Stage II through the entire Stage III, elevated C_{org}/P_{reac} above the canonical Redfield ratio of 106/1, coincident with rising $\delta^{138}Ba_{carb}$ (Figure 2b), indicates significantly intensified P regeneration and its return to surface waters via upwelling, fueling pelagic productivity (Figures 3a and 3b). Moreover, the marked Hg (and Hg_{corr}) anomalies at the N-CIE onset (Figure 2b) suggest intensified volcanism and associated aeolian delivery of volcanogenic material to this pelagic site (Figure 3a), representing a close analog to ash-fall fertilization recorded in pelagic settings during the Permian–Triassic mass extinction interval from eruptions of the Siberian Traps (Grasby et al., 2024). The persistently elevated Hg through the middle N-CIE recovery interval (Figure 2b) indicates continued dust-borne fertilization, which, together with upwelling-derived nutrients, could have assisted in sustaining a protracted high level of pelagic productivity (Figure 3b).

To quantitatively evaluate the impacts of sustained high pelagic productivity on the carbon cycle and marine redox during the T-OAE, we here calculated the OC burial rate at Dogna and further estimated the total amount of OC buried in the Belluno Trough Basin through the event. In detail, given the potential carbonate dilution effect, we first corrected the bulk TOC data at Dogna (see Section 2 above), with an average OC_{corr} of 2.13 wt.% through the T-OAE N-CIE interval (Table S1 in Supporting Information S1). Subsequently, utilizing a duration of ~300 kyr for the T-OAE N-CIE interval based on the latest high-precision geochronology (Kemp, Ramezani, et al., 2024) and 17.56 m (28.01–10.45 m core depth) in thickness for the T-OAE N-CIE strata at Dogna, we calculated an average linear sedimentation rate of ~5.85 cm/kyr at this pelagic site through the event. Combined

with a typical rock density of 2.7 g cm^{-3} (Owens et al., 2018), the OC burial rate at Dogna was then calculated as the product of average OC_{corr}, linear sedimentation rate, and rock density, yielding a rate of ~3.37 g C m^{-2} y^{-1} during the T-OAE. Given a rough estimate of the area of the Belluno Trough Basin (~10,000 km^2 assuming 50 km in width and 200 km in length; Picotti & Cobianchi, 2017), the total amount of OC buried in this narrow and elongated basin was perhaps as much as ~10 Gt C.

OC-rich facies are also commonly observed in other pelagic settings of the Alpine-Mediterranean Tethys, including the Lombardy Basin, Italy (Erba et al., 2022; Gambacorta et al., 2024; Jenkyns, 1988), the Pindos Zone and Ionian Zone, Greece (Jenkyns, 1988; Kafousia et al., 2011, 2014), the Bächental Basin, Austria (Suan et al., 2016), and the Úrkút Basin, Hungary (Suan et al., 2016). At the Austro-Alpine sector along the open NW Tethyan margin, approximately 179 Gt of OC and 478 Gt of sulfur were buried through the event (Suan et al., 2018). Furthermore, high TOC content (>30 wt.%) and pyrite enrichments (pyrite sulfur concentrations of 10 wt.%) are recorded in the central Panthalassic Ocean (Chen et al., 2022, 2023; Ikeda et al., 2018; Kemp, Chen, et al., 2022), with broadly comparable OC-rich and sulfidic conditions also reported from the eastern Panthalassic deeper waters (Them et al., 2018). Taken together, pelagic environments may have played a significant role in OC burial or storage in oceans (e.g., dissolved OC), assisting in regulating the climatic perturbations and oceanic deoxygenation during the T-OAE.

4. Conclusions

Our $\delta^{138}Ba_{carb}$ records from a shallow-water carbonate platform (Nianduo) and a pelagic basin (Dogna) reveal a coherent increase in marine productivity at the T-OAE N-CIE onset, indicating a supra-regional biological response to initial climatic and environmental forcings. Following this early phase, productivity evolution diverged strongly between depositional settings. The shallow carbonate platform experienced only a short-lived productivity enhancement linked to weathering-driven terrigenous nutrient availability, whereas the pelagic basin maintained elevated productivity for a longer interval extending well into the N-CIE recovery phase due to the continued supply of upwelling-derived nutrients and aeolian fertilization. This productivity contrast highlights fundamental differences in how shallow- and deep-marine systems responded to large-scale climatic perturbations. Sustained high productivity and efficient OC burial in the pelagic basin imply that deep-marine environments made an important contribution to carbon sequestration during the T-OAE.

Conflict of Interest

The authors declare no conflicts of interest relevant to this study.

Availability Statement

All data reported in this paper can be accessed in the Supplementary Information and are also available via Chen, W (2026) at Mendeley Data (https://data.mendeley.com/datasets/gcydkkyh88/2).

Acknowledgments
This study is supported by the National Natural Science Foundation of China Program (Grant 42425002), the National Key Research & Development Program of China (Grant 2023YFF0804000), and the National Natural Science Foundation of China Program (Grant 42302119). We thank Zihu Zhang for his assistance in the laboratory. We are grateful to Dr Alex Dickson and Dr S. Hohl for their constructive comments that greatly improved the manuscript.

References

Bellanca, A., Masetti, D., Neri, R., & Venezia, F. (1999). Geochemical and sedimentological evidence of productivity cycles recorded in Toarcian black shales from the Belluno Basin, Southern Alps, Northern Italy. *Journal of Sedimentary Research*, *69*(2), 466–476. https://doi.org/10.2110/jsr.69.466

Bosellini, A., Masetti, D., & Sarti, M. (1981). A Jurassic "Tongue of the ocean" infilled with oolitic sands: The Belluno Trough, Venetian Alps, Italy. *Marine Geology*, *44*(1–2), 59–95. https://doi.org/10.1016/0025-3227(81)90113-4

Bridgestock, L., Hsieh, Y. T., Porcelli, D., & Henderson, G. M. (2019). Increased export production during recovery from the Paleocene–Eocene thermal maximum constrained by sedimentary Ba isotopes. *Earth and Planetary Science Letters*, *510*, 53–63. https://doi.org/10.1016/j.epsl.2018.12.036

Bridgestock, L., Nathan, J., Paver, R., Hsieh, Y. T., Porcelli, D., Tanzil, J., et al. (2021). Estuarine processes modify the isotope composition of dissolved riverine barium fluxes to the ocean. *Chemical Geology*, *579*, 120340. https://doi.org/10.1016/j.chemgeo.2021.120340

Canfield, D. E., Bjerrum, C. J., Zhang, S., Wang, H., & Wang, X. (2020). The modern phosphorus cycle informs interpretations of Mesoproterozoic Era phosphorus dynamics. *Earth-Science Reviews*, *208*, 103267. https://doi.org/10.1016/j.earscirev.2020.103267

Canfield, D. E., Lyons, T. W., & Raiswell, R. (1996). A model for iron deposition to euxinic Black Sea sediments. *American Journal of Science*, *296*(7), 818–834. https://doi.org/10.2475/ajs.296.7.818

Chen, W. (2026). Data for: Barium isotopes indicate spatiotemporal heterogeneity of marine primary productivity during the Toarcian Oceanic Anoxic Event. *Mendeley Data, V2*. https://doi.org/10.17632/gcydkkyh88.2

Chen, W., Kemp, D. B., He, T., Newton, R. J., Xiong, Y., Jenkyns, H. C., et al. (2023). Shallow- and deep-ocean Fe cycling and redox evolution across the Pliensbachian–Toarcian boundary and Toarcian Oceanic Anoxic Event in Panthalassa. *Earth and Planetary Science Letters*, *602*, 117959. https://doi.org/10.1016/j.epsl.2022.117959

Chen, W., Kemp, D. B., Jenkyns, H. C., Robinson, S. A., Jiang, S., Pan, C., & Li, C. (2024). Widespread upper-ocean deoxygenation in the Alpine-Mediterranean Tethys during the Toarcian Oceanic Anoxic Event. *Global and Planetary Change*, *243*, 104631. https://doi.org/10.1016/j.gloplacha.2024.104631

Chen, W., Kemp, D. B., Newton, R. J., He, T., Huang, C., Cho, T., & Izumi, K. (2022). Major sulfur cycle perturbations in the Panthalassic Ocean across the Pliensbachian-Toarcian boundary and the Toarcian Oceanic Anoxic Event. *Global and Planetary Change*, *215*, 103884. https://doi.org/10.1016/j.gloplacha.2022.103884

Clarkson, M. O., Poulton, S. W., Guilbaud, R., & Wood, R. A. (2014). Assessing the utility of Fe/Al and Fe-speciation to record water column redox conditions in carbonate-rich sediments. *Chemical Geology*, *382*, 111–122. https://doi.org/10.1016/j.chemgeo.2014.05.031

Cohen, A. S., Coe, A. L., Harding, S. M., & Schwark, L. (2004). Osmium isotope evidence for the regulation of atmospheric CO_2 by continental weathering. *Geology*, *32*(2), 157–160. https://doi.org/10.1130/G20158.1

Dera, G., & Donnadieu, Y. (2012). Modeling evidences for global warming, Arctic seawater freshening, and sluggish oceanic circulation during the Early Toarcian anoxic event. *Paleoceanography*, *27*(2), PA211. https://doi.org/10.1029/2012PA002283

Erba, E., Cavalheiro, L., Dickson, A. J., Faucher, G., Gambacorta, G., Jenkyns, H. C., & Wagner, T. (2022). Carbon-and oxygen-isotope signature of the Toarcian Oceanic Anoxic Event: Insights from two Tethyan pelagic sequences (Gajum and Sogno Cores–Lombardy Basin, northern Italy). *Newsletters on Stratigraphy*, *55*(4), 451–477. https://doi.org/10.1127/nos/2022/0690

Ettinger, N. P., Larson, T. E., Kerans, C., Thibodeau, A. M., Hattori, K. E., Kacur, S. M., & Martindale, R. C. (2021). Ocean acidification and photic-zone anoxia at the Toarcian Oceanic Anoxic Event: Insights from the Adriatic Carbonate Platform. *Sedimentology*, *68*(1), 63–107. https://doi.org/10.1111/sed.12786

Farrimond, P., Stoddart, D. P., & Jenkyns, H. C. (1994). An organic geochemical profile of the Toarcian anoxic event in northern Italy. *Chemical Geology*, *111*(1–4), 17–33. https://doi.org/10.1016/0009-2541(94)90080-9

Fendley, I. M., Frieling, J., Mather, T. A., Ruhl, M., Hesselbo, S. P., & Jenkyns, H. C. (2024). Early Jurassic large igneous province carbon emissions constrained by sedimentary Mercury. *Nature Geoscience*, *17*(3), 241–248. https://doi.org/10.1038/s41561-024-01378-5

Froelich, P. N., Klinkhammer, G. P., Bender, M. L., Luedtke, N. A., Heath, G. R., Cullen, D., et al. (1979). Early oxidation of organic matter in pelagic sediments of the eastern equatorial Atlantic: Suboxic diagenesis. *Geochimica et Cosmochimica Acta*, *43*(7), 1075–1090. https://doi.org/10.1016/0016-7037(79)90095-4

Gambacorta, G., Brumsack, H. J., Jenkyns, H. C., & Erba, E. (2024). The early Toarcian Oceanic Anoxic Event (Jenkyns Event) in the Alpine-Mediterranean Tethys, North African margin, and North European epicontinental seaway. *Earth-Science Reviews*, *248*, 104636. https://doi.org/10.1016/j.earscirev.2023.104636

Gill, B. C., Lyons, T. W., & Jenkyns, H. C. (2011). A global perturbation to the sulfur cycle during the Toarcian Oceanic Anoxic Event. *Earth and Planetary Science Letters*, *312*(3–4), 484–496. https://doi.org/10.1016/j.epsl.2011.10.030

Grasby, S. E., Ardakani, O. H., Liu, X., Bond, D. P., Wignall, P. B., & Strachan, L. J. (2024). Marine snowstorm during the Permian–Triassic mass extinction. *Geology*, *52*(2), 120–124. https://doi.org/10.1130/G51497.1

Grasby, S. E., Them, T. R., Chen, Z., Yin, R., & Ardakani, O. H. (2019). Mercury as a proxy for volcanic emissions in the geologic record. *Earth-Science Reviews*, *196*, 102880. https://doi.org/10.1016/j.earscirev.2019.102880

Han, Z., Hu, X., Li, J., & Garzanti, E. (2016). Jurassic carbonate microfacies and relative sea-level changes in the Tethys Himalaya (southern Tibet). *Palaeogeography, Palaeoclimatology, Palaeoecology*, *456*, 1–20. https://doi.org/10.1016/j.palaeo.2016.05.012

Han, Z., Hu, X., Hu, Z., Jenkyns, H. C., & Su, T. (2022). Geochemical evidence from the Kioto Carbonate Platform (Tibet) reveals enhanced terrigenous input and deoxygenation during the early Toarcian. *Global and Planetary Change*, *215*, 103887. https://doi.org/10.1016/j.gloplacha.2022.103887

Han, Z., Hu, X., Kemp, D. B., & Li, J. (2018). Carbonate-platform response to the Toarcian Oceanic Anoxic Event in the southern hemisphere: Implications for climatic change and biotic platform demise. *Earth and Planetary Science Letters*, *489*, 59–71. https://doi.org/10.1016/j.epsl.2018.02.017

Hesselbo, S. P., Gröcke, D. R., Jenkyns, H. C., Bjerrum, C. J., Farrimond, P., Bell, H. S. M., & Green, O. R. (2000). Massive dissociation of gas hydrate during a Jurassic oceanic anoxic event. *Nature*, *406*(6794), 392–395. https://doi.org/10.1038/35019044

Horner, T. J., Kinsley, C. W., & Nielsen, S. G. (2015). Barium-isotopic fractionation in seawater mediated by barite cycling and oceanic circulation. *Earth and Planetary Science Letters*, *430*, 511–522. https://doi.org/10.1016/j.epsl.2015.07.027

Hsieh, Y. T., & Henderson, G. M. (2017). Barium stable isotopes in the global ocean: Tracer of Ba inputs and utilization. *Earth and Planetary Science Letters*, *473*, 269–278. https://doi.org/10.1016/j.epsl.2017.06.024

Hua, X., Yin, R., Kemp, D. B., Huang, C., Shen, J., & Jin, X. (2023). Mercury isotope constraints on the timing and pattern of magmatism during the end-Triassic mass extinction. *Earth and Planetary Science Letters*, *624*, 118438. https://doi.org/10.1016/j.epsl.2023.118438

Ikeda, M., Hori, R. S., Ikehara, M., Miyashita, R., Chino, M., & Yamada, K. (2018). Carbon cycle dynamics linked with Karoo-Ferrar volcanism and astronomical cycles during Pliensbachian-Toarcian (Early Jurassic). *Global and Planetary Change*, *170*, 163–171. https://doi.org/10.1016/j.gloplacha.2018.08.012

Jacobsen, S. B., & Kaufman, A. J. (1999). The Sr, C and O isotopic evolution of Neoproterozoic seawater. *Chemical Geology*, *161*(1–3), 37–57. https://doi.org/10.1016/S0009-2541(99)00080-7

Jenkyns, H. C. (1988). The early Toarcian (Jurassic) anoxic event-stratigraphic, sedimentary, and geochemical evidence. *American Journal of Science*, *288*(2), 101–151. https://doi.org/10.2475/ajs.288.2.101

Jenkyns, H. C. (2010). Geochemistry of oceanic anoxic events. *Geochemistry, Geophysics, Geosystems*, *11*(3), Q03004. https://doi.org/10.1029/2009GC002788

Jenkyns, H. C., Géczy, B., & Marshall, J. D. (1991). Jurassic manganese carbonates of central Europe and the early Toarcian anoxic event. *The Journal of Geology*, *99*(2), 137–149. https://doi.org/10.1086/629481

Jenkyns, H. C., Gröcke, D. R., & Hesselbo, S. P. (2001). Nitrogen isotope evidence for water mass denitrification during the early Toarcian (Jurassic) oceanic anoxic event. *Paleoceanography*, *16*(6), 593–603. https://doi.org/10.1029/2000PA000558

Jenkyns, H. C., Sarti, M., Masetti, D., & Howarth, M. K. (1985). Ammonites and stratigraphy of Lower Jurassic black shales and pelagic limestones from the Belluno Trough, Southern Alps, Italy. *Eclogae Geologicae Helvetiae*, *78*, 299–311. https://doi.org/10.5169/seals-26716

Jin, C., Li, C., Algeo, T. J., Planavsky, N. J., Cui, H., Yang, X., et al. (2016). A highly redox-heterogeneous ocean in South China during the early Cambrian (~529–514 Ma): Implications for biota-environment co-evolution. *Earth and Planetary Science Letters*, *441*, 38–51. https://doi.org/10.1016/j.epsl.2016.02.019

Kafousia, N., Karakitsios, V., Jenkyns, H. C., & Mattioli, E. (2011). A global event with a regional character: The Early Toarcian Oceanic Anoxic Event in the Pindos Ocean (northern Peloponnese, Greece). *Geological Magazine*, *148*(4), 619–631. https://doi.org/10.1017/S0016756811000082

Kafousia, N., Karakitsios, V., Mattioli, E., Kenjo, S., & Jenkyns, H. C. (2014). The Toarcian Oceanic Anoxic event in the Ionian Zone, Greece. *Palaeogeography, Palaeoclimatology, Palaeoecology*, *393*, 135–145. https://doi.org/10.1016/j.palaeo.2013.11.013

Kemp, D. B., Chen, W., Cho, T., Algeo, T. J., Shen, J., & Ikeda, M. (2022). Deep-ocean anoxia across the Pliensbachian-Toarcian boundary and the Toarcian Oceanic Anoxic Event in the Panthalassic Ocean. *Global and Planetary Change*, *212*, 103782. https://doi.org/10.1016/j.gloplacha.2022.103782

Kemp, D. B., Han, Z., Hu, X., Chen, W., Jin, S., Izumi, K., et al. (2024). Global hydroclimate perturbations during the Toarcian oceanic anoxic event. *Earth-Science Reviews*, *258*, 104946. https://doi.org/10.1016/j.earscirev.2024.104946

Kemp, D. B., Ramezani, J., Izumi, K., Al-Suwaidi, A., Huang, C., Chen, W., & Zhu, Y. (2024). The timing and duration of large-scale carbon release in the Early Jurassic. *Geology*, *52*(12), 891–895. https://doi.org/10.1130/G52457.1

Kemp, D. B., Selby, D., & Izumi, K. (2020). Direct coupling between carbon release and weathering during the Toarcian oceanic anoxic event. *Geology*, *48*(10), 976–980. https://doi.org/10.1130/G47509.1

Kemp, D. B., Suan, G., Fantasia, A., Jin, S., & Chen, W. (2022). Global organic carbon burial during the Toarcian oceanic anoxic event: Patterns and controls. *Earth-Science Reviews*, *231*, 104086. https://doi.org/10.1016/j.earscirev.2022.104086

Lin, Y., Wei, H., Jiang, S., Hohl, S., Lei, H., Liu, X., & Dong, G. (2020). Accurate determination of barium isotopic compositions in sequentially leached phases from carbonates by double spike-thermal ionization mass spectrometry (DS-TIMS). *Analytical Chemistry*, *92*(3), 2417–2424. https://doi.org/10.1021/acs.analchem.9b03137

Lin, Y., Wei, H., Zhang, F., Hohl, S. V., Wei, G., Li, T., et al. (2022). Evaluation of shallow-water corals and associated carbonate sediments as seawater Ba isotope archives in the South China Sea. *Palaeogeography, Palaeoclimatology, Palaeoecology*, *605*, 111196. https://doi.org/10.1016/j.palaeo.2022.111196

Mavromatis, V., Goetschl, K. E., Grengg, C., Konrad, F., Purgstaller, B., & Dietzel, M. (2018). Barium partitioning in calcite and aragonite as a function of growth rate. *Geochimica et Cosmochimica Acta*, *237*, 65–78. https://doi.org/10.1016/j.gca.2018.06.018

Mavromatis, V., van Zuilen, K., Purgstaller, B., Baldermann, A., Nägler, T. F., & Dietzel, M. (2016). Barium isotope fractionation during witherite ($BaCO_3$) dissolution, precipitation and at equilibrium. *Geochimica et Cosmochimica Acta*, *190*, 72–84. https://doi.org/10.1016/j.gca.2016.06.024

Mayfield, K. K., Horner, T. J., Torfstein, A., Auro, M. E., Crockford, P. W., & Paytan, A. (2024). Barium cycling in the Gulf of Aqaba. *Frontiers in Earth Science*, *12*, 1178487. https://doi.org/10.3389/feart.2024.1178487

Nan, X., Yu, H., Rudnick, R. L., Gaschnig, R. M., Xu, J., Li, W., et al. (2018). Barium isotopic composition of the upper continental crust. *Geochimica et Cosmochimica Acta*, *233*, 33–49. https://doi.org/10.1016/j.gca.2018.05.004

Newton, R. J., Reeves, E. P., Kafousia, N., Wignall, P. B., Bottrell, S. H., & Sha, J. G. (2011). Low marine sulfate concentrations and the isolation of the European Epicontinental Sea during the Early Jurassic. *Geology*, *39*(1), 7–10. https://doi.org/10.1130/G31326.1

Owens, J. D., Lyons, T. W., & Lowery, C. M. (2018). Quantifying the missing sink for global organic carbon burial during a Cretaceous oceanic anoxic event. *Earth and Planetary Science Letters*, *499*, 83–94. https://doi.org/10.1016/j.epsl.2018.07.021

Pálfy, J., & Smith, P. L. (2000). Synchrony between Early Jurassic extinction, oceanic anoxic event, and the Karoo-Ferrar flood basalt volcanism. *Geology*, *28*(8), 747–750. https://doi.org/10.1130/0091-7613(2000)28<747:SBEJEO>2.0.CO;2

Paytan, A., & McLaughlin, K. (2007). The oceanic phosphorus cycle. *Chemical Reviews*, *107*(2), 563–576. https://doi.org/10.1021/cr0503613

Pedersen, T. F., & Calvert, S. E. (1990). Anoxia vs. productivity: What controls the formation of organic-carbon-rich sediments and sedimentary rocks? *AAPG Bulletin*, *74*(4), 454–466. https://doi.org/10.1306/0C9B232B-1710-11D7-8645000102C1865D

Percival, L. M. E., Witt, M. L. I., Mather, T. A., Hermoso, M., Jenkyns, H. C., Hesselbo, S. P., et al. (2015). Globally enhanced Mercury deposition during the end-Pliensbachian extinction and Toarcian OAE: A link to the Karoo–Ferrar Large Igneous Province. *Earth and Planetary Science Letters*, *428*, 267–280. https://doi.org/10.1016/j.epsl.2015.06.064

Picotti, V., & Cobianchi, M. (2017). Jurassic stratigraphy of the Belluno Basin and Friuli Platform: A perspective on far-field compression in the Adria passive margin. *Swiss Journal of Geosciences*, *110*(3), 833–850. https://doi.org/10.1007/s00015-017-0280-5

Poulton, S. W. (2021). The iron speciation paleoredox proxy. In *Elements in geochemical tracers in Earth system science* (p. 75). Cambridge University Press.

Schoepfer, S. D., Shen, J., Wei, H., Tyson, R. V., Ingall, E., & Algeo, T. J. (2015). Total organic carbon, organic phosphorus, and biogenic barium fluxes as proxies for paleomarine productivity. *Earth-Science Reviews*, *149*, 23–52. https://doi.org/10.1016/j.earscirev.2014.08.017

Storm, M. S., Hesselbo, S. P., Jenkyns, H. C., Ruhl, M., Al-Suwaidi, A. H., Percival, L. M. E., et al. (2024). Integrated stratigraphy of Pliensbachian and Toarcian strata from the northern Neuquén Basin, Argentina. *Newsletters on Stratigraphy*, *57*(4), 389–415. https://doi.org/10.1127/nos/2024/0817

Suan, G., Schlögl, J., & Mattioli, E. (2016). Bio- and chemostratigraphy of the Toarcian organic-rich deposits of some key successions of the Alpine Tethys. *Newsletters on Stratigraphy*, *49*(3), 401–419. https://doi.org/10.1127/NOS/2016/0078

Suan, G., Schöllhorn, I., Schlögl, J., Segit, T., Mattioli, E., Lécuyer, C., & Fourel, F. (2018). Euxinic conditions and high sulfur burial near the European shelf margin (Pieniny Klippen Belt, Slovakia) during the Toarcian oceanic anoxic event. *Global and Planetary Change*, *170*, 246–259. https://doi.org/10.1016/j.gloplacha.2018.09.003

Them, T. R., Gill, B. C., Caruthers, A. H., Gerhardt, A. M., Gröcke, D. R., Lyons, T. W., et al. (2018). Thallium isotopes reveal protracted anoxia during the Toarcian (Early Jurassic) associated with volcanism, carbon burial, and mass extinction. *Proceedings of the National Academy of Sciences*, *115*(26), 6596–6601. https://doi.org/10.1073/pnas.1803478115

Them, T. R., Gill, B. C., Selby, D., Gröcke, D. R., Friedman, R. M., & Owens, J. D. (2017). Evidence for rapid weathering response to climatic warming during the Toarcian Oceanic Anoxic Event. *Scientific Reports*, *7*(1), 5003. https://doi.org/10.1038/s41598-017-05307-y

Them, T. R., Jagoe, C. H., Caruthers, A. H., Gill, B. C., Grasby, S. E., Gröcke, D. R., et al. (2019). Terrestrial sources as the primary delivery mechanism of Mercury to the oceans across the Toarcian Oceanic Anoxic Event (Early Jurassic). *Earth and Planetary Science Letters*, *507*, 62–72. https://doi.org/10.1016/j.epsl.2018.11.029

Thompson, J., Poulton, S. W., Guilbaud, R., Doyle, K. A., Reid, S., & Krom, M. D. (2019). Development of a modified SEDEX phosphorus speciation method for ancient rocks and modern iron-rich sediments. *Chemical Geology*, *524*, 383–393. https://doi.org/10.1016/j.chemgeo.2019.07.003

Wei, G., Chen, T., Poulton, S. W., Lin, Y., He, T., Shi, X., et al. (2021). A chemical weathering control on the delivery of particulate iron to the continental shelf. *Geochimica et Cosmochimica Acta*, *308*, 204–216. https://doi.org/10.1016/j.gca.2021.05.058

Wei, G., Ling, H., Shields, G. A., Hohl, S. V., Yang, T., Lin, Y., & Zhang, F. (2021). Revisiting stepwise ocean oxygenation with authigenic barium enrichments in marine mudrocks. *Geology*, *49*(9), 1059–1063. https://doi.org/10.1130/G48825.1

Yang, Y., Han, Z., Hu, X., He, T., Newton, R. J., & Harvey, J. (2024). Strontium isotope evidence for regional enhanced continental weathering during the early Toarcian in the Tethys Himalaya. *Palaeogeography, Palaeoclimatology, Palaeoecology*, *641*, 112136. https://doi.org/10.1016/j.palaeo.2024.112136

Yu, Y., Xie, R. C., Gutjahr, M., Laukert, G., Cao, Z., Hathorne, E., et al. (2022). High latitude controls on dissolved barium isotope distributions in the global ocean. *Geochemical Perspectives Letters*, *24*, 22–26. https://doi.org/10.7185/geochemlet.2242

Zhang, F., Pohl, A., Elrick, M., Wei, G., Cheng, K., Crockford, P., et al. (2025). Enhanced marine biological pump as a trigger for the onset of the late Paleozoic ice age. *Science Advances*, *11*(27), eadv2756. https://doi.org/10.1126/sciadv.adv2756

Zhang, F., Xiong, G., Wei, G., Lin, Y., Li, X., & Shen, S. (2024). Barium isotopes constrain the triggering mechanism of the Cretaceous OAE 2 in the Neotethys Ocean. *Earth and Planetary Science Letters*, *646*, 118990. https://doi.org/10.1016/j.epsl.2024.118990

References From the Supporting Information

Algeo, T. J., & Ingall, E. (2007). Sedimentary C_{org}: P ratios, paleocean ventilation, and Phanerozoic atmospheric pO_2. *Palaeogeography, Palaeoclimatology, Palaeoecology*, *256*(3–4), 130–155. https://doi.org/10.1016/j.palaeo.2007.02.029

Bodin, S., Mattioli, E., Fröhlich, S., Marshall, J. D., Boutib, L., Lahsini, S., & Redfern, J. (2010). Toarcian carbon isotope shifts and nutrient changes from the Northern margin of Gondwana (High Atlas, Morocco, Jurassic): Palaeoenvironmental implications. *Palaeogeography, Palaeoclimatology, Palaeoecology*, *297*(2), 377–390. https://doi.org/10.1016/j.palaeo.2010.08.018

Fantasia, A., Föllmi, K. B., Adatte, T., Bernárdez, E., Spangenberg, J. E., & Mattioli, E. (2018). The Toarcian oceanic anoxic event in south-western Gondwana: An example from the Andean Basin, northern Chile. *Journal of the Geological Society*, *175*(6), 883–902. https://doi.org/10.1144/jgs2018-008

Geyman, B. M., Ptacek, J. L., LaVigne, M., & Horner, T. J. (2019). Barium in deep-sea bamboo corals: Phase associations, barium stable isotopes, & prospects for paleoceanography. *Earth and Planetary Science Letters*, *525*, 115751. https://doi.org/10.1016/j.epsl.2019.115751

Jadoul, F., Berra, F., & Garzanti, E. (1998). The Tethys Himalayan passive margin from Late Triassic to Early Cretaceous (South Tibet). *Journal of Asian Earth Sciences*, *16*(2–3), 173–194. https://doi.org/10.1016/S0743-9547(98)00013-0

Masetti, D., Fantoni, R., Romano, R., Sartorio, D., & Trevisani, E. (2012). Tectonostratigraphic evolution of the Jurassic extensional basins of the eastern Southern Alps and Adriatic foreland based on an integrated study of surface and subsurface data. *AAPG Bulletin*, *96*(11), 2065–2089. https://doi.org/10.1306/03091211087

Ruebsam, W., Reolid, M., Marok, A., & Schwark, L. (2020). Drivers of benthic extinction during the early Toarcian (Early Jurassic) at the northern Gondwana paleomargin: Implications for paleoceanographic conditions. *Earth-Science Reviews*, *203*, 103117. https://doi.org/10.1016/j.earscirev.2020.103117

Ruttenberg, K. C. (1992). Development of a sequential extraction method for different forms of phosphorus in marine sediments. *Limnology & Oceanography*, *37*(7), 1460–1482. https://doi.org/10.4319/lo.1992.37.7.1460

Schlachter, T. A., & Connolly, R. M. (2014). Effects of acid treatment on carbon and nitrogen stable isotope ratios in ecological samples: A review and synthesis. *Methods in Ecology and Evolution*, *5*, 541–550. https://doi.org/10.1111/2041-210X.12183

Wang, Y., Sun, D., & He, G. (1980). New advances in the stratigraphy of the Chinese part of the Himalayas. *Journal of Stratigraphy*, *4*, 55–59. (in Chinese with English abstract).

Winterer, E. L., & Bosellini, A. (1981). Subsidence and sedimentation on Jurassic passive continental margin. *AAPG Bulletin*, *65*(3), 394–421. https://doi.org/10.1306/2F9197E2-16CE-11D7-8645000102C1865D

Yin, J. R. (2010). *Jurassic ammonites of Tibet* (p. 247). Geological Publishing House. in Chinese with English abstract.